Article:

Zhang, B. and Marshall, M.B. (2018) Investigating the Application of a Honeycomb Abradable Lining in the Turbine Stage of an Aero-Engine. Tribology International, 125. pp. 66-74. ISSN 0301-679X

https://doi.org/10.1016/j.triboint.2018.04.013

Abstract

Modern aero-engines use abradable linings to reduce axial gas leakage. In this study the wear performance of a new developed nickel superalloy honeycomb abradableliningwas investigated on a novel high-speed test rig, using in-situ measurement techniques, combined with post-test microscopy and X-ray fluorescence based elemental analysis. In particular the effect of changing the nickel-aluminide filler ratio was considered, as well as the impact of thermal ageing of the specimens. Compaction of abradable occurs, resulting in fin wear, along with high forces and temperatures. This wear mechanism is cyclic with debris ejection and sparks. Ageing of the abradable generally leads to an increase in fin wear, with the exception that in one case this lead to improved fracture of the abradable and an improved cutting performance by the fin.

1 Introduction

In an aero engine, axial gas flow in the gaps between the rotating blade tips and the surrounding casing leads to reduced thermal efficiency, causing increased operating costs and CO_2 emissions. Therefore aero engine operators aim to minimise this gap and keep it as small as possible in order to minimise leakage. This is achieved by using abradable linings [1], into which the blade tips cut, producing a seal for a given engine stage.

Abradable linings are applied in both the compressor and turbine stages of the engine with different sealing systems. Generally, the compressor blade is in direct contact with the abradable lining, whereas a T-shaped tooth, which is also called a turbine blade fin, is used to shroud the turbine blade. In the latter case, the tip of the tooth is in contact with the lining. [2, 3]

Further, as aero-engines continue to develop, higher core temperatures are required to improve overall performance. This leads to higher working temperatures in the turbine stage of the engine, and in particular in the high-pressure turbine. These temperatures are beyond the operating limit of traditional thermally sprayed abradables [4, 5], and honeycomb based materials have been developed, consisting of a nickel alloyed honeycomb structure and nickel-aluminium filler [6, 7]. These materials have been designed to be resistive to the higher operating temperatures required.

Recently, researchers have been investigating the use of abradables in aero-engines, with Oerlikon Metco focusing on researching and manufacturing materials for gas turbine applications [3, 6, 7, 8]. They conducted a series of studies investigating the use of different abradables such as aluminium-silicon and nickel based systems for different coating applications. The performances of the different systems were linked to material properties, along with working temperature and operating speed. In particular the wear mechanisms at each of these operating conditions were identified. A series of studies have also been undertaken to characterize the wear mechanism between an abradable lining and compressor blade using in-situ measurement techniques. These techniques have included stroboscopic imaging to analyse the adhesive transfer between the blade tips and lining [9], as well as contact force measurement [10], and have been used to investigate the effect of different blade tip treatments [11] and abradable hardness [12] on the wear mechanics. Compared to compressor blade tip and abradable interactions, limited studies are available with respect to sealing fins. Delebarre et al. investigated the fin seal system for an Inconel 718 triple-fin blade and Al-Si abradable [13]. In their study, tests with low incursion rate showed cyclical behaviour in terms of force and material removal; however no reason was given for this behaviour. Apart from this latter study, no other studies are present in the literature on sealing fines.

The aim of this study is to explore the wear mechanism between Inconel 718 fins and nickel-aluminium honeycomb abradables, by evaluating the wear behaviour during an incursion test. In particular the effect of the filler composition will be investigated, as well as the impact of thermal ageing on the samples. Post-test, microscope and X-ray fluorescence (XRF) analysis will be used on the rub area in order to understand the wear mechanism between the fin tip and different honeycomb abradables, and combined with the in-situ measurements.

2 Material and Method

2.1 Test rig

This study uses a test rig previously developed at the University of Sheffield to study the wear mechanism between aero-engine linings and compressor blades or turbine fin tips [14]. The rig consists of a rotating disc driven by a high-speed spindle, and a microscope stage (OptoSigma SHOT-202, Laser2000 UK Ltd., Northants, UK) onto which the abradable sample is mounted (Figure 1a). Within the disc two fin samples are mounted, with one being used as the sample for test, and the other a dummy for balancing. The spindle is capable of rotating the disc up to speeds of 21000RPM, with this corresponding to a blade tip speed of 200ms^{-1}. Similarly, the microscope stage can operate with a linear speed between 0.1 and 2000 μms^{-1}. The rig is operated by a customized Labview programme, and an incursion event is created by moving the abradable sample towards the rotating disc at a set speed, until a prescribed depth is reached.

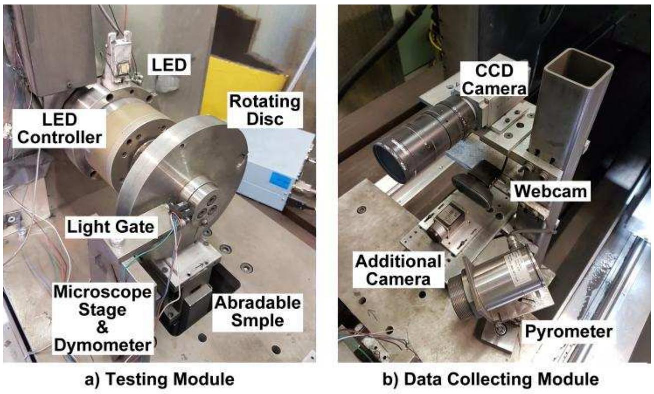

Figure 1 Testing& Data Collect modules on test rig

The sensor system on the test rig (Figure 1b) consists of a CCD camera (Pixelink PL-B741U, Scorpion Vision Ltd., Hants., UK), a webcam (Logitech C90, Logitech International S.A., Switzerland), a dynamometer (3-Component Force Link Type 9317C, Kistler Instruments Ltd. UK) and a pyrometer (Optris CTXL3MH1-CF3, Optris GmbH, Germany). The CCD camera uses an LED stroboscopic imaging system (9) to capture the fin profile during the test, and is powered by an impulse power source. A small metal arm fixed onto the rotating disc interrupts a light gate linked to the imaging system, and in this way the timing of the flash can be set, and the camera used to capture an image of the fin when it passes top dead centre. Additionally, the webcam takes video of the sparks and the screenshots are saved automatically every 50ms by the LabView programme. The dynamometer is installed under the abradable sample. It measures the force magnitude during the test and transfers the signal to the computer. Finally, the inferred pyrometer focuses on the abradable samples and passes the real-time temperature reading of the wear area to the computer.

2.2 Test sample andtest parameters

The abradable samples used in this study consisted of a nickel superalloy honeycomb structure with nickel aluminide filler (Figure 2a). The first three samples were in the un-aged condition and had a standard, nickel rich and aluminium rich filler respectively. The nickel-aluminium powder, which is also called nickel aluminide, has two phases, NiAl and Ni_3Al; and these phases shift with different nickel contents[15]. Generally, Ni_3Al is harder and has lower thermal conductivity than NiAl [16-18], and it is also important to note that NiAl transforms to Ni_3Al under high temperature [19]. The standard filler has a Ni-Al weight ratio of 86%-14% [5], which is typically used in aero-engines. The second set of samples have the same honeycomb structure and filler combinations, but this time are in the aged condition, to compare the effect of the ageing process. The ageing process is conducted by heating as-manufactured samples continually for 100 hours under 1000°C to simulate the real-life engine working environment. Following exposure to high temperature, the nickel aluminide is oxidised and produces $NiAl_2O_4$[20]. $NiAl_2O_4$ has a spinel structure that leads to a very high level of hardness and very low thermal conductivities [21, 22].

Figure 2 Standard un-aged honeycomb abradable and HVOF coated Inconel718 Fin

The fin sample (Figure 2b) used in this study is made from Inconel 718, is 30mm in length, flat with 3mm thickness, and with the fin tip tapered to 1.3mm to simulate the turbine fin geometry. Generally, the turbine blades and the sealing fins in aero-engines are made from Inconel 718, which is the same as the material used in this study. Additionally, the samples are coated with ZrO_2 by a HVOF coating method in order to emulate the real aero-engine. In an aero-engine, the turbine blades are usually coated by different coating materials for different aims. The most common coating type is a thermal barrier coating, which can protect the blade fin from thermal damage. ZrO_2 combined with Al_2O_3 is a common thermal barrier coating material due to its low thermal conductivity [23]. This coating material can be coated onto the blade fin surface by using plasma electrolytic oxidation [24) or high velocity oxygen fuel spraying (HVOF) [25].

Test Code	Fin Type	Abradable	Tip Speed [m/s]	Incursion speed [μm/s]	Incursion Rate [μm/pass]	Incursion Depth [μm]

Test - S	IN718-HVOF	Standard	200	62.1	0.2	2500
Test - A,S	IN718-HVOF	Aged standard	200	62.1	0.2	2500
Test - Al+	IN718-HVOF	Aluminium rich	200	62.1	0.2	2500
Test - A,Al+	IN718-HVOF	Aged aluminium rich	200	62.1	0.2	2500
Test - Ni+	IN718-HVOF	Nickel rich	200	62.1	0.2	2500
Test - A,Ni+	IN718-HVOF	Aged nickel rich	200	62.1	0.2	2500

Table 1 Designed testing parameters

As previously introduced, this study is focused on how the abradable filler properties affect the wear mechanism between the fin tip and abradable. Additionally, according to previous research, the tip speed and incursion speed are two dominant parameters with respect to the wear mechanism but the incursion depth is not a dominant test parameter [9-12]. Therefore, all the tests are conducted with a tip speed of 200ms^{-1} and incursion speed of 62.1μms^{-1}. It should be noted that the incursion speed is selected to represent the incursion rate of 0.2μm/pass that was used in previous research [10, 12] and is aero-engine representative. The incursion depth for this study was set at 2500μm to ensure that the test duration is sufficient for collecting data that would allow full analysis of the wear mechanism. Table 1shows the test conditions of each test, with a test code for the nickel-aluminium content (S: standard, Al+: aluminium rich and Ni+: nickel rich) and ageing condition (A: aged) used to label all tables and figures in this paper.

2.3 Test procedure anddata processing

As previously detailed, there are two slots on the rotation disc for fitting the fin samples. The dummy fin sample, made from IN718 is 3mm shorter than the testing sample, and was fixed onto the rotation disc by clamps in one slot. The fin sample to be tested is then fitted into the other slot. After the abradable is fixed on the microscope stage, the test is conducted. During the test, all test conditions are controlled by the LabView programme. Additionally, the programme captures live videos from the webcam cameras and saves the frames individually for post-processing. The data from the dynamometer and pyrometer is also saved individually in a text format with a timestamp.

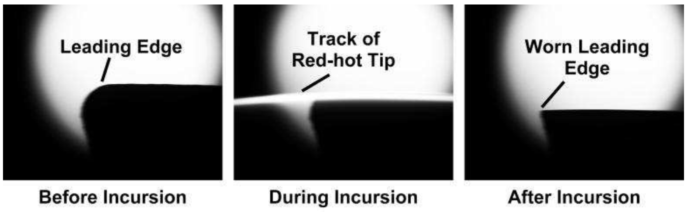

Figure 3 Fin profile during testing

The change in the length of the fin can be determined by analysing the images captured by the CCD camera (Figure 3). Each image contains four or five exposures of the fin tip profile due to the high rotation speed, as it is much higher than the camera stroboscopic frequency. The other set of images captured come from the fin-abradable contact and show the interaction. As the honeycomb abradable is relatively hard, a spark is generated by the wear process, and shown on the webcam monitor (Figure 4) with data captured at a frequency of 50ms.

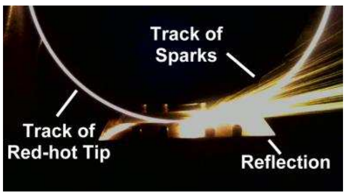

Figure 4 Sparking during testing with aged standard abradable

Since the fin is running in a circular route during the test, the force magnitude in the axial direction is always zero. Therefore, the dynamometer outputs two sets of force data, which represent the radial (normal) and tangential force components. The dynamometer outputs are processed into a single data set that presents the force change against time by extracting the maximum force recorded from each strike. In a similar manner, temperature data is also recorded as a function of time.

Wear occurs as the fin passes over the abradable surface, with the arc of contact increasing as the incursion depth of the fin into the abradable increases. As the time for each rotation of the disc is constant during the test, the total rub length does not linearly relate to the test time. Therefore in order to compare the results, the total rub length was calculated, as this is reflective of the work done by the fin on the abradable, and is calculated as follows:

$$\mathbf{L} = \sum_{i=1}^{n} \cos^{-1}\left(\frac{r - incursionrate \times i \times 10^{-6}}{r}\right) \times r$$

where L is counted total rub length (m), r is the fin disk radius (m), and i is the number of pass.

All outputs obtained from the test rig are processed into five individual characteristic variables, fin length, normal force, tangential force, temperature and sparks change along with the total rub length.

The worn groove is also investigated post-test. To study the difference between each groove, microscopic and X-Ray fluorescence (XRF) analyses were employed on the worn groove surface. The microscope used was a Carl Zeiss Imager A1.M optical microscope with 5.0x zoom-in coefficient, with three images taken (one in the middle point and two at the end points) of each wear scar. The XRF test was conducted using a Fischerscope X-Ray fluorescence machine (Fischerscope X-Ray XAN-250, Fischer Technology Inc., USA), which detects the elemental content of a material sample surface within a small round area of 1.2mm diameter. To reduce the error, ten sample points are randomly taken from the detecting surface for repeat testing and the result is the average value of these ten data sets. Finally, the test samples were sectioned at the middle of the wear groove to analyse the sub-surface structure.

3 Results

During the testing procedure, the incursion depth was changed twice (Table 2). As mentioned in the previous section, the incursion depth was originally set at 2500μm. However, during testing of both the standard and aged standard abradables high fin wear was detected, and led to the disc becoming unbalanced. Therefore for the two subsequent tests, the incursion depth was reduced to 1000μm, in order to avoid damage to the spindle. After testing the two aluminium rich abradables at this depth, the incursion depth was increased to 1500μm for the remaining two nickel rich abradable samples, as the level of expected fin wear was now understood. Increasing the test duration led to more data being collected. However, upon analysis it was determined that all tests, even those of shorter durations, had run for a sufficient amount of time to be both steady state and create a data set that could be fully analysed.

Test Code	Fin Type	Abradable	Tip Speed [ms-1]	Incursion Rate [μm/pass]	Incursion Depth [μm]
Test - S	IN718-HVOF	Standard	200	0.2	2500
Test - A,S	IN718-HVOF	Aged standard	200	0.2	2500
Test - Al+	IN718-HVOF	Aluminium rich	200	0.2	1000
Test - A,Al+	IN718-HVOF	Aged aluminium rich	200	0.2	<1000
Test - Ni+	IN718-HVOF	Nickel rich	200	0.2	1500
Test - A,Ni+	IN718-HVOF	Aged nickel rich	200	0.2	1500

Table 2 Actual testing parameters

3.1 Worn groove analysis

The most direct evidence for determining the wear performance during the test is the worn groove. Figure 5 shows the wear scar on each of the abradables and fins after the test. Also marked on the figure is the expected groove length in each case, and by comparing this to the actual groove length achieved, an indication of wear can be seen. Where the worn groove is similar in value to that expected, fin wear was low, and where the actual groove is significantly shortened, high wear is observed. As shown in the Figure 5, the performance of the standard, aged standard and aged nickel rich abradables was poor during the test, and that the only test to achieve close to the expected groove length was the un-aged nickel rich sample.

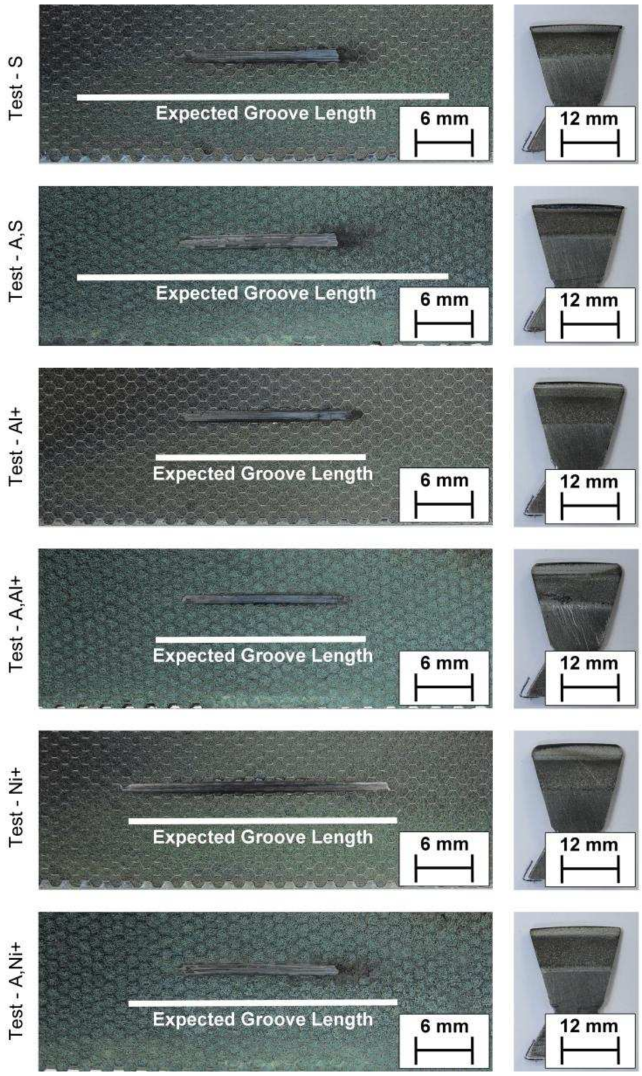

Figure 5 Worn groove and fin profile after testing

3.2 In-cycle measurements

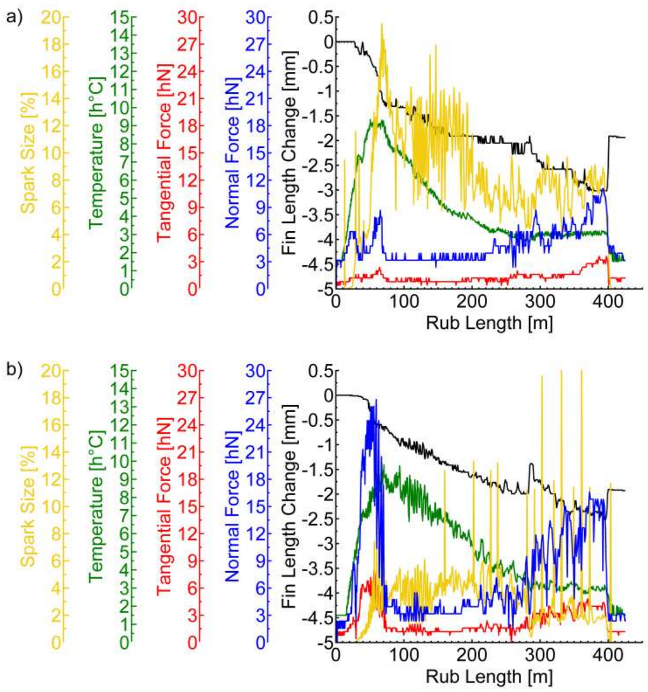

Figure 6 Test results for standard abradables, a) Test - S b) Test – A,S

Figure 6 shows the fin length change, force (normal and tangential), temperature and spark results from the standard and the aged-standard tests. These results have been selected as they contain features typical of the different incursion tests. As shown, after the start of the test the force and temperature at the contact point increase and reach a peak value around a rub length of 50 to 60 meters. During this event the fin length begins to shorten, and just prior to the force and temperature reducing, a spark (represented by the spark size) is released. As shown in Figure 6b, in some cases cyclic behaviour is also observed with this process repeated periodically during the test. In other cases, as shown Figure 6a, the test is more stable with less peaks in the force and temperature data. However, in the latter case it should be noted that sparks continue to be emitted.

When comparing across the different tests, for the un-aged abradable the most significant sparking was observed in the standard case, with this being accompanied by the largest blade length change. At the other extreme, the nickel rich abradable was extremely consistent with comparatively low forces and temperatures (650°C), with negligible blade wear and sparking observed. In the case of the aged abradables, forces and temperatures were higher than when compared to the un-aged case, with an increased tendency for cyclic behaviour. An exception was the test with the aged aluminium rich specimen, where no sparking was observed, and fin wear was minimal (Figure 5).

3.3 Post-processed results

Further numerical analysis was applied to all the incursion test results in order to compare the different tests more directly. The fin wear condition was quantitatively analysed by measuring the fin length and weight before and after the test (shown in Figure 7). However, as noted, the total rub lengths were different between tests, meaning that further processing of results was required to make a valid comparison. Previous research has shown that material loss is proportional to rub length for abradable material [10]. Therefore in order to compare between the six tests, the fin length and weight change was normalised with respect to total rub length, and is similarly shown on Figure 7. As shown in Figure 7, both standard and aged standard abradables suffer significant wear damage as does the aged nickel rich one. It should also be noted that even though there is no fin length change observed after the test with nickel rich abradable, the fin weight is slightly reduced. As shown in Figure 5, in this case the loss of material can be seen on the leading edge of the fin tip, where the tip coating is slightly removed due to wear. As a general point, the fins tested with aluminium rich abradables tend to experience less wear, with this especially true for the aged case.

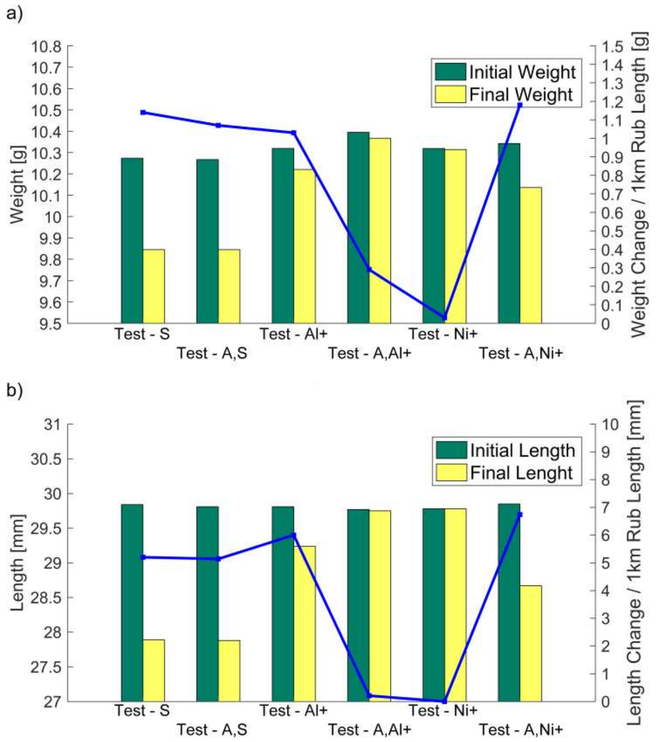

Figure 7 Fin weight change before and after incursion test

The maximum force and temperature data were extracted from the steady state test results to evaluate the difference between each test (Figure 8). With regards to force, it can be observed that the maximum tangential forces of the tests with aged abradables are higher than the un-aged ones. The temperature results also suggest that more frictional heating is generated during the tests with aged abradables. It is also interesting to note that there is more variation in the force results for the aged abradables than compared to the un-aged case; where with the exception of the normal force for the standard un-aged abradable, normal forces are similar for all the filler types, as are the tangential forces.

As will be discussed later, the link between force and temperature is complicated, as changing the aluminium-nickel ratio in the filler changes the thermal diffusivity and mechanical properties. For example, the nickel rich abradable has relatively high forces, but lower temperatures when compared to the other tests. However, what is clear is that upon ageing a given abradable, both the force and temperature rise, suggesting that additional frictional heating occurs.

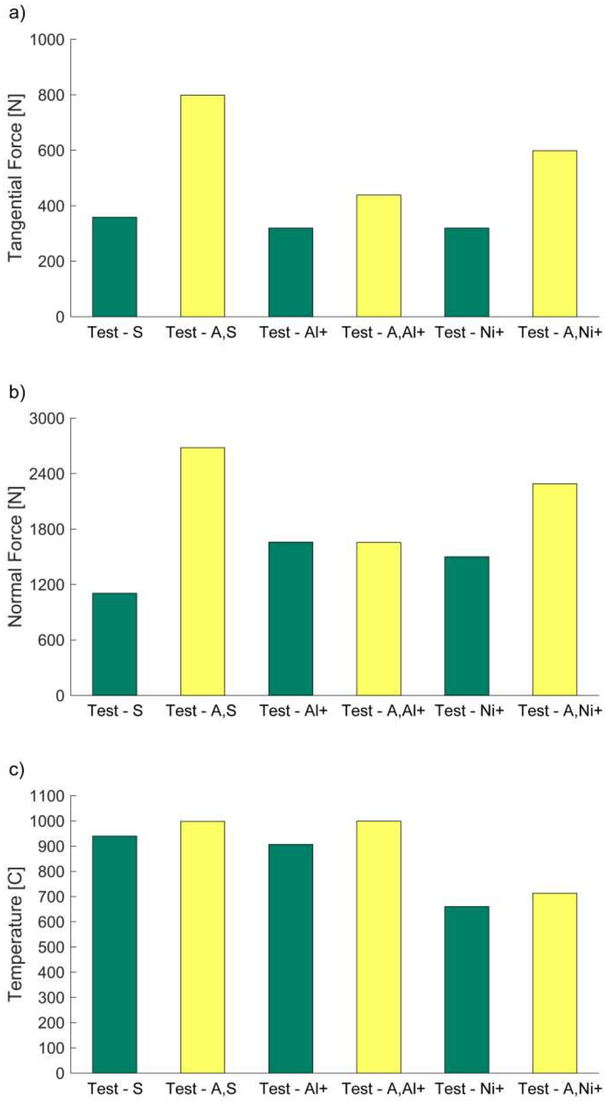

Figure 8 Comparison of maximumforce and temperature

4 Post-test characterization

4.1 Worn groove surface micrographic analysis

Whilst the variable rub lengths in the tests created the need for further processing of the fin length and weight change results, this was not an issue when analysing the wear scars as in each case the wear mechanism was fully developed. Figure 9 shows the microscope images of the different surfaces of the worn grooves. It can be seen that compared to the other three worn grooves, those of the aluminium rich, aged aluminium rich and nickel rich abradables are relatively smooth and shiny. Additionally, data from the incursion test results shows that these three abradables have lower fin wear. On the other hand, the worn grooves of the standard, aged standard and aged nickel rich abradables are rough; these worn grooves contain shiny and dark surfaces. It was also observed during the microscope analysis that the shiny layer is above the dark layer. Finally, all of the worn grooves have areas containing blue-purple marks on the surface, which represent thermal damage to the material.

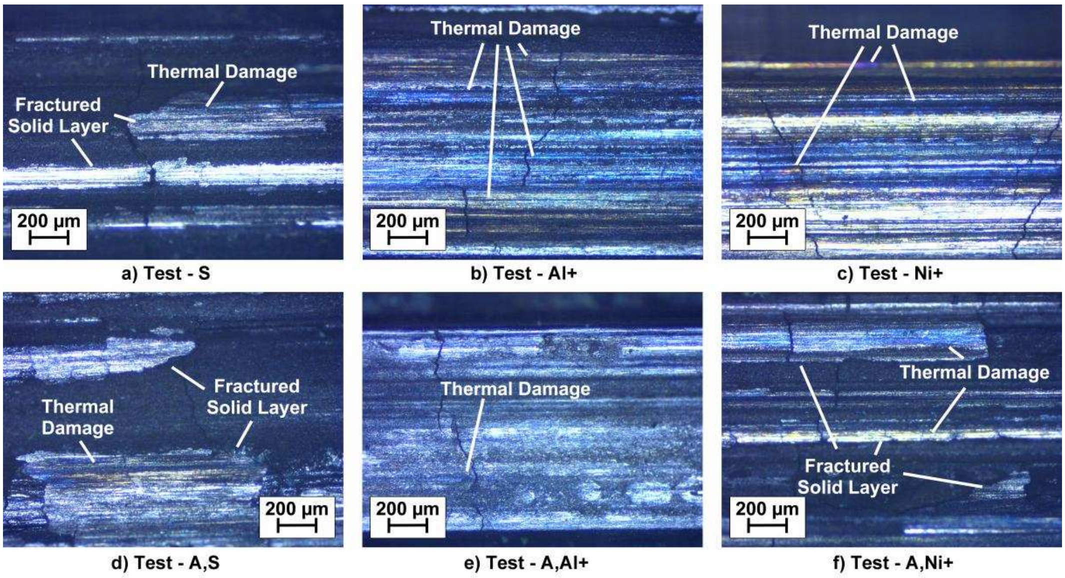

Figure 9 Microscopies (5.0x)of worn grooves surface

4.2 X-ray fluorescence (XRF)

XRF investigation (Table 3) of the fin and the abradable samples highlighted that nickel and zirconium can be defined as characteristic elements, and used to determine whether the rub track on a sample is material from the abradable or also made up of transfer from the fin. As shown in the Table 3, the abradable sample is made up of over 90% nickel, compared to 47% for the base material of the fin, with the only source of zirconium being the fin tip. As previously highlighted, a smooth surfaceto some degree is seen in all of the samples apart from the un-aged Nickel rich one. The rub tracks on these samples contain a mixture of nickel and zirconium, with the nickel concentration being at a lower percentage than the base abradable. This indicates that the smooth surface is a consolidated mixture of the abradable and the fin material. As was also mentioned, the groove surface on the nickel rich abradable is unique. The elemental distribution of this sample is very close to that of base abradable material, indicating negligible transfer from the fin in this case.

Test Code	Ti	Cr	Fe	Co	Ni[1]	Cu	Zr	Nb	Mo	Ta	Balance
Test - S	0.81	14.35	17.92	1.21	57.75	0.08	0.68	4.16	2.78	0.26	0.00
Test - A,S	0.97	18.03	18.09	0.56	53.12	0.09	0.83	5.61	2.52	0.19	-0.01
Test - Al+	0.96	19.74	18.11	0.64	50.22	0.08	2.00	5.58	2.48	0.20	-0.01
Test - A,Al+	1.39	25.16	14.71	1.71	47.89	0.16	3.14	3.72	1.81	0.31	0.00
Test - Ni+	0.00	3.51	3.34	0.38	90.19	0.06	0.00	0.05	1.92	0.27	0.28
Test - A,Ni+	0.97	18.23	17.77	1.03	52.03	0.07	1.34	6.00	2.39	0.18	-0.01
Fin Base	0.95	16.69	17.33	0.17	47.53	8.17	0.17	5.45	3.07	0.48	-0.01
Fin Tip	0.00	1.27	0.00	2.61	3.37	0.07	82.66	0.00	0.51	0.00	9.51
Abradable[2]	0.04	5.36	1.65	0.23	90.46	0.08	0.00	0.05	1.87	0.29	-0.03

Table 3 XRF results for abradable groove surface, blade and un-tested abradable

4.3 Worn groove sectional micrographic analysis

The test samples were also sectioned, with Figure 10 presenting the sectioned views of the worn grooves from each test. As shown in the Figure 10, the aged samples are significantly discoloured due to oxidation, when compared to their un-aged counterparts. For the un-aged samples, the morphology of the grooves shows there are two main components in each case, a surface layer of consolidated material that may or may not be partially removed, with a sub-layer of compressed filler beneath it. However, it should also be noted that the nickel rich sample is unusual in the sense that the surface layer negligible with minimum compaction of the filler. This result is in line with the XRF measurement for this sample (see section 4.2), where the elemental distribution was close to that of the base material. Comparing the standard and aluminium rich specimens, in the former case the consolidated layer is prone to fracture and removal, whereas in the latter case higher levels of distortion are present with a more continuous layer formed.

[1]Fischerscope® X-Ray XAN®-250 cannot detect aluminium element therefore the nickel content in the table represents sum of aluminium and nickel content.
[2] The abradable XRF result present the average value of six different abradable

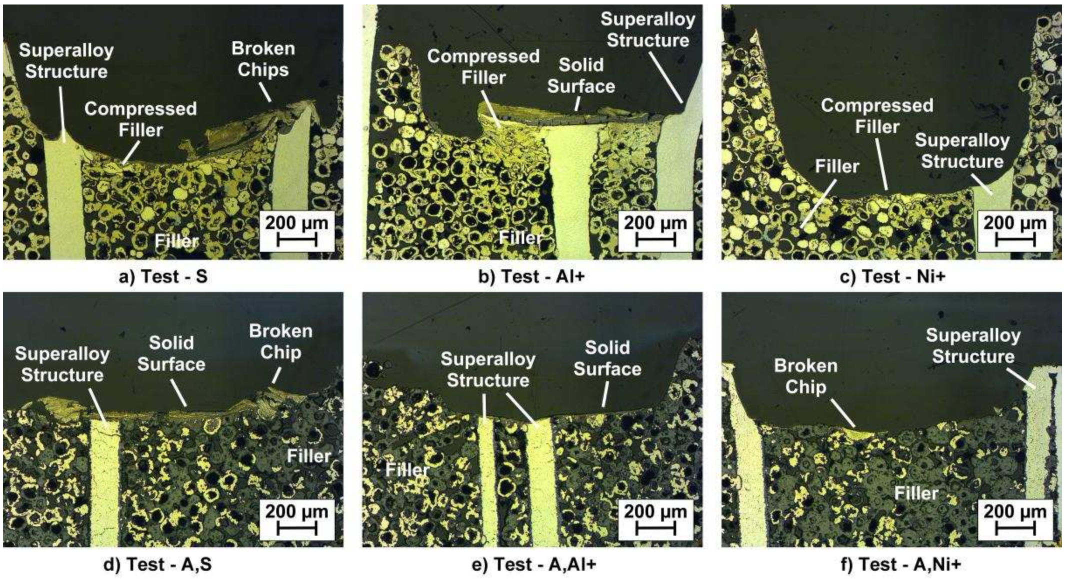

Figure 10 Microscopies (5.0x) of sectional viewing of worn grooves

For the aged samples, with the exception of the aged standard case, the surface layer is less significant, with the compressed layer also less apparent. Indeed, whilst evident from the images of the rub tracks (Figure 9), the consolidated layer is only really evident in the sectioned view of the aged standard abradable. It is also interesting to note, for this sample as in the un-aged case, fracture and removal of the consolidated layer occurs. With respect to the aluminium and nickel rich aged specimens, the consolidated material is minimal, and confined to a very thin surface layer, although as highlighted by the XRF measurements, fin transfer occurs.

5 Discussion

The results of the incursion tests give both insights into the mechanism of material removal, as well as showing clear differences between each condition investigated. In this section the material removal mechanism will be discussed, as well as the influence of both the nickel-aluminium ratio in the filler and ageing.

5.1 Material removal mechanism

As highlighted in the results section, cyclic behaviour in terms of force and temperature has been observed, coupled with sparking. This behaviour occurred in the tests with standard, aged standard and aged nickel rich abradables, and was similar in nature to that observed in previous studies [13]. As shown by the microscope images in section 4.1, the groove surfaces on these abradables is coarse, with the microscopic images presented in section 4.3 suggesting that this type of surface is made up of two layers. The upper layer is shiny, with XRF results suggesting that the shiny layer is consolidated material from both the abradable and fin tip. The lower layer is rough, and has a relatively dark colour, and has been identified as the filler in a compressed powder form. Further, the fractured nature of the upper layer also indicates it cracks and periodically peels off, resulting in the observed coarsely worn surface.

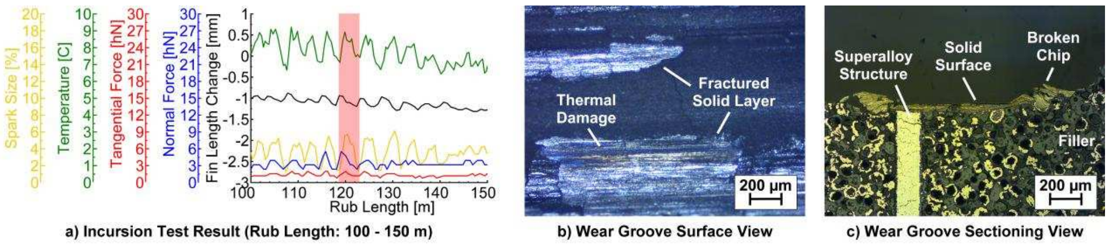

Figure 11 General results of incursion test with aged standard abradable

Combining these observations with the cyclic force and temperature behaviour recorded during tests, the sparking mechanism can be divided into four steps, and is summarised in Figure 11. Taking the aged standard abradable as an example, initially the fin tip touches the abradable surface and the abradable is compacted. This results in high forces and frictional heating as the material is compressed, leading to a hard dense metal layer containing a mixture of fin and abradable material. As the incursion progresses, force and temperature continue to rise, until at a certain point ductility in the compacted layer is exceeded and fracture occurs. The solid surface then splits into small hot chips and is peeled away due to the high forces, resulting in sparks. The ejection of material then leads to a gap, force and temperature reduce, and consolidation re-initiates, with this process repeatable over the duration of the test. In the cases where this process does not occur or is lesser in severity, such as the nickel rich case, it is due to fracture of the abradable and an absence of consolidating behaviour.

5.2 Influence of Ni/Al ratio & ageing

As highlighted in the results section a range of different behaviours were observed for the honeycomb samples. Significant differences were observed linked to the Ni-Al ratio as well as whether the samples were aged or not. As previously highlighted, the abradable filler is a nickel-aluminium powder that creates a Ni-Al matrix system. In a Ni-Al matrix system, changing the Ni-Al ratio leads to significantly different material properties [15]. For un-aged (as manufactured) abradables, a higher nickel concentration gives an increased percentage of Ni_3Al, while a higher aluminium concentration leads to a higher percentage of NiAl [15], with the standard case having a mixture of the two. These changes are significant, as Ni_3Al in particular is hard, brittle, and has poor thermal diffusivity [18].

The effect of these changes is evident in the test samples. In the case of the standard sample, forces and temperatures are relatively high, with significant compaction and brittle fracture of the consolidated layer. When the aluminium ratio is increased, as in the aluminium rich case, the softer abradable consolidates significantly more (Figure 10b). Whilst it might be expected that temperatures and forces are reduced compared to the standard case, as the material is softer and with increased thermal diffusivity [17], this is not the case. The increased level of consolidation leads to significant push back and frictional heating, resulting in higher fin wear, force and temperatures than seen for the standard ratio. With regards to fin wear, temperature is a significant factor, as Inconel 718 will soften at temperatures over 700°C [26], highlighting why wear may be higher for the softer aluminium rich case. Conversely, it might be expected that for the nickel rich case, the harder filler of lower thermal diffusivity will be worse. However, as observed, good fracture of the abradable occurs with little consolidation (Figure 10c). Whilst forces are still relatively high due to the hardness of the filler, temperatures and fin wear are reduced in the absence of a significantly compacted layer. This latter case highlights how the compacted layer drives the wear mechanics of the system.

Further changes occur to the nickel-aluminium filler with ageing, as the filler oxidises. Upon oxidation, both NiO and a spinel structured $NiAl_2O_4$ phase are generated [20]. The $NiAl_2O_4$ phase in particular is of increased hardness, brittle and of reduced thermal diffusivity [21]. Generally ageing leads to a decrease in wear performance, as the abradable is now harder, except in the aluminium rich case where a change in mechanism occurs.

In the case of the standard aged sample, it has mixture of NiO and $NiAl_2O_4$ phases, leading to high forces and temperatures, along with fin wear. For the aluminium rich aged specimen wear is reduced. In this case, the increased aluminium ratio leads to a higher concentration of the $NiAl_2O_4$ phase. As this phase is relatively brittle, increased fracture of the abradable occurs and consolidation is reduced. Whilst temperatures are relatively high due to the poor thermal diffusivity of this material, driving some blade wear, forces are lower due to the absence of significant consolidation, and the overall performance improved when compared to the standard case. Finally, for the nickel rich aged sample, the NiO phase dominates, and is accompanied by high forces and moderate temperatures, with temperatures reduced compared to the standard case due to the improved thermal diffusivity of NiO compared to $NiAl_2O_4$.

Overall the ability of the filler to fracture has the most significant impact on the performance of the honeycomb aluminium-nickel filled abradable system. In the un-aged case, the nickel rich sample fractures well and shows the best performance, whereas in the aged condition this occurs in the aluminium rich case. As the abradable ages in the engine, the aluminium rich abradable offers the best long term performance, however, pre-ageing is required in order to avoid negative wear performance during initial running of the engine.

6 Conclusions

This project mainly studied the wear mechanism between the IN718-HVOF blade and different nickel-aluminium based abradables. The results from the wear test and the other analyses show that:

- The fin typically compacts the abradable, frequently leading to a dense surface. This surface layer leads to high forces and temperatures, and ultimately fractures resulting in the release of sparks on a cyclic basis.
- Different Ni-Al content of the filler leads to different hardness and brittleness which affects the fracture behaviour of the abradable. Generally, the fin is less worn when the abradable is easy to fracture.
- The ageing process hardens the abradable samples and changes the thermal diffusivity, resulting in changes to the wear mechanisms observed then compared to un-aged tests.
- High aluminium content makes abradable hard to fracture under as-manufactured condition but easy to fracture after ageing.

REFERENCES

[1] D. Sporer, A. Refke, M. Dratwinski, M. Dorfman, Sulzer Metco plc., I. Giovannetti, M. Giannozzi, M. Bigi, GE Oil&Gas plc., New high-temperature seal system - Increased efficiency of gas turbine. 2008, Sulzer Technical Review, 2/2008. DOI: 10.1016/S1350-4789(08)70517-8

[2] W. Dalzell, S. Sanders, G. Crawford, F. Walden, W. Woodard, Abradable seal with improved properties.US 6352264, USA, 2002.

[3] S. Wilson OerlikonMetco, Thermally sprayed abradable coating technology for sealing in gas turbines. 2012, Brussels. Available at: https://www.oerlikon.com/ecomaXL/files/oerlikon_ThermallySprayedAbradableCoatings_2012.10.pdf&download=1 [Accessed 5 Mar. 2018].

[4] Oerlikon Metco, Material Product Data Sheet - Aluminum Silicon Hexagonal Boron Nitride Abradable. 2014. Available at: https://www.oerlikon.com/ecomaXL/files/oerlikon_DSMTS-0017.3_AlSi-hBN.pdf&download=1 [Accessed 5 Mar. 2018].

[5] Oerlikon Metco, Material Product Data Sheet - Aluminum Silicon Polymer Thermal Spray Powders. 2016. Available at: https://www.oerlikon.com/ecomaXL/files/metco/oerlikon_DSMTS-0016.6_AlSi-Poly.pdf&download=1 [Accessed 5 Mar. 2018].

[6] Oerlikon Metco AG, Improve efficiency and reduce emissions with high pressure turbine abradable coatings for industrial gas turbines. 2014. SF-0015.1.

[7] Oerlikon Metco, Material Product Data Sheet - Nickel Aluminum for Sintered Abradable Honeycomb Fillers. 2014. Available at: https://www.oerlikon.com/ecomaXL/files/oerlikon_DSMB-0051.4_NiAl_Honeycomb.pdf&download=1 [Accessed 5 Mar. 2018].

[8] Sulzer Metco Plc., Solutions Flash - Improve efficiency and reduce emissions with high pressure turbine abradable coatings for industrial gas turbines. 2012. Available at: https://www.oerlikon.com/ecomaXL/files/oerlikon_SF-0015.1_IGT_HPT_Abradables_EN.pdf&download=1 [Accessed 5 Mar. 2018].

[9] N. Fois, J. Stringer, J and M. Marshall, Adhesive transfer in aero-engine abradable linings contact, 2013, Wear, Vol. 304, No. 1-2, pp. 202-210.Wear304(2013)202–210. DOI: 10.1016/j.wear.2013.04.033

[10] N. Fois, M. Watson, J. Stringer,M. Marshall, An investigation of the relationship between wear and contact force for abradable materials. 2014, Proceedings of the Institution of Mechanical Engineers, Part J: Journal of Engineering Tribology, Vol. 229, No. 2, pp. 136-150.DOI: 10.1177/1350650114545139

[11] M. Watson, N. Fois, M. Marshall,Effects of blade surface treatments in tip–shroud abradable contacts, 2015, Wear, Vol. 338-339, pp. 268-281.DOI: 10.1016/j.wear.2015.06.018

[12] N. Fois, M. Watson, M. Marshall, The influence of material properties on the wear of abradable materials, 2016, Proceedings of the Institution of Mechanical Engineers, Part J: Journal of Engineering Tribology. DOI: 10.1177/1350650116649528

[13] C. Delebarre, V. Wagner, J. Paris, G. Dessein, J. Denape, J. Gurt-Santanach, An experimental study of the high speed interaction between a labyrinth seal and an abradable coating in a turbo-engine application. 2014, Wear, Vol. 316, No. 1-2, pp. 109-118. DOI: 10.1016/j.wear.2014.04.023

[14] J. Stringer,M. Marshall, High speed wear testing of an abradable coating. 2012, Wear, Vol. 294-295, pp. 257-263. DOI: 10.1016/j.wear.2012.07.009

[15] G. Dey,Physical metallurgy of nickel aluminides, 2003, Sadhana, Vol. 28, No. 1-2, pp. 247-262. DOI: 10.1007/BF02717135

[16] D. Kaliński, M. Chmielewski, K.Pietrzak, Mechanical, thermal and tribological properties of hot-pressed NiAl-Al2O3 composites. 2012, 15th European conference on composite materials, ECCM15.

[17] J. Guo, Z. Wang, L. Sheng, L. Zhou, C. Yuan, Z. Chen, Z, L. Song, Wear properties of NiAl based materials. 2012, Progress in Natural Science: Materials International, Vol. 22, No. 5, pp. 414-425. DOI: 10.1016/j.pnsc.2012.10.008

[18] P. Jozwik, W. Polkowski, Z. Bojar,Applications of Ni_3Al Based Intermetallic Alloys—Current Stage and Potential Perceptivities, 2015, Materials, Vol. 8, No. 5, pp. 2537-2568. DOI: 10.3390/ma8052537

[19] Y. Tamarin, Protective coatings for turbine blades. 2002, Materials Park, Ohio: ASM International, pp. 86.ISBN: 978-0-87170-759-8

[20] E. Loginova, F.Cosandey, T.Madey,Nanoscopic nickel aluminate spinel ($NiAl_2O_4$) formation during NiAl (111) oxidation, 2007, Surface Science, Vol. 601, No. 3, pp L11-L14. DOI: 10.1016/j.susc.2006.11.047

[21] Y. He, K. Shih,Nano-indentation on nickel aluminate spinel and the influence of acid and alkaline attacks on the spinel surface, 2012, Ceramics International, Vol. 38, No. 4, pp. 3121-3128. DOI: 10.1016/j.ceramint.2011.12.013

[22] J. Zygmuntowicz, P.Wiecińska, A. Miazga,K.Konopka, Characterization of composites containing $NiAl_2O_4$ spinel phase from Al_2O_3/NiO and Al_2O_3/Ni systems. 2016, Journal of Thermal Analysis and Calorimetry, Vol. 125, No. 3, pp. 1079-1086. DOI: 10.1007/s10973-016-5357-2

[23] J. Hostaša, W. Pabst, J. Matějíček, Thermal Conductivity of Al_2O_3-ZrO_2 Composite Ceramics, 2011, Journal of the American Ceramic Society, Vol. 94, No. 12, pp. 4404-4409. DOI: 10.1111/j.1551-2916.2011.04875.x

[24] T. Akatsu, T. Kato, Y. Shinoda,F. Wakai, Thermal barrier coating made of porous zirconium oxide on a nickel-based single crystal superalloy formed by plasma electrolytic oxidation, 2013, Surface and Coatings Technology, Vol. 223, pp. 47-51. DOI: 10.1016/j.surfcoat.2013.02.026

[25] T. Dobbins, R. Knight, M. Mayo, HVOF Thermal Spray Deposited Y2O3-Stabilized ZrO2 Coatings for Thermal Barrier Applications, 2003, Journal of Thermal Spray Technology, Vol. 12, No. 2, pp. 214-225. DOI: 10.1361/105996303770348320

[26] Special Metals, Product handbookof high-performance alloys, 2008.

Figure 1

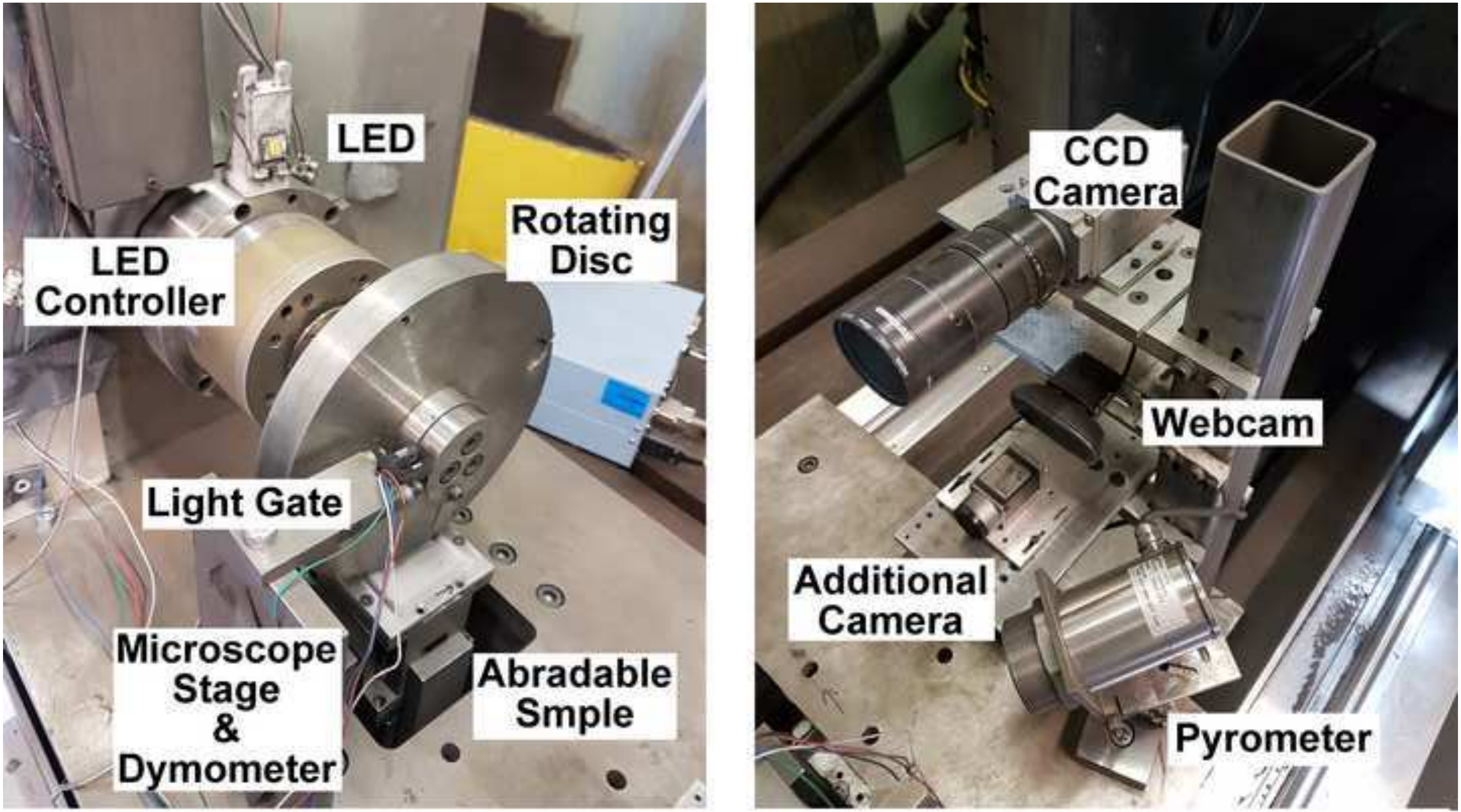

a) Testing Module   b) Data Collecting Module

Figure 2

a) Honeycomb Abradable Sample

b) Fin Sample

Figure 3

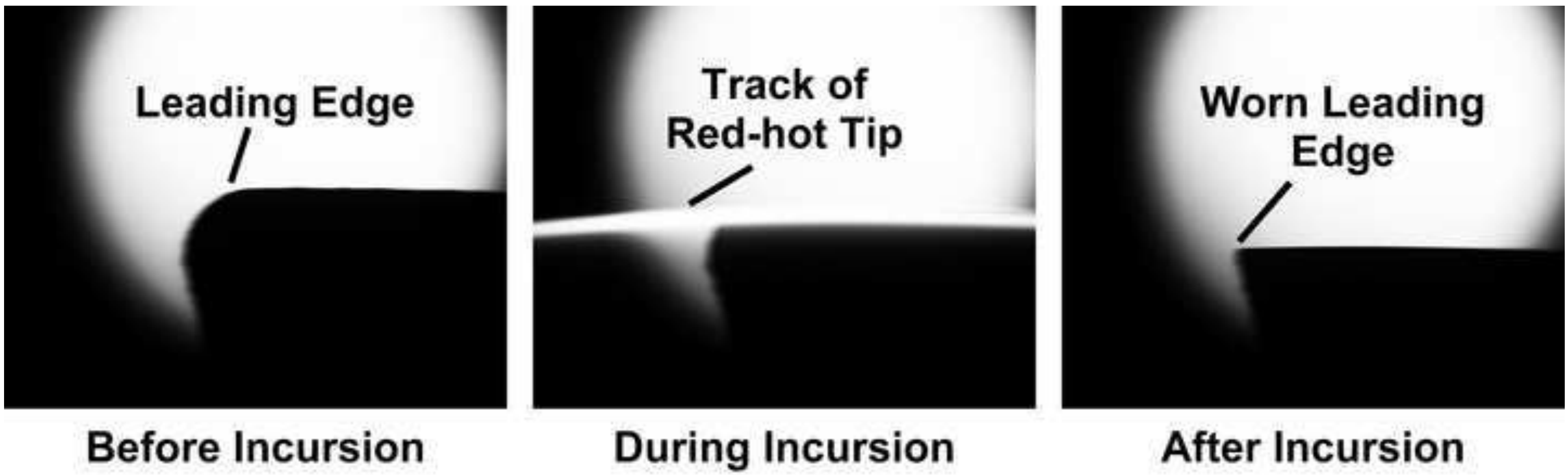
Leading Edge
Track of Red-hot Tip
Worn Leading Edge
Before Incursion
During Incursion
After Incursion

Figure 4

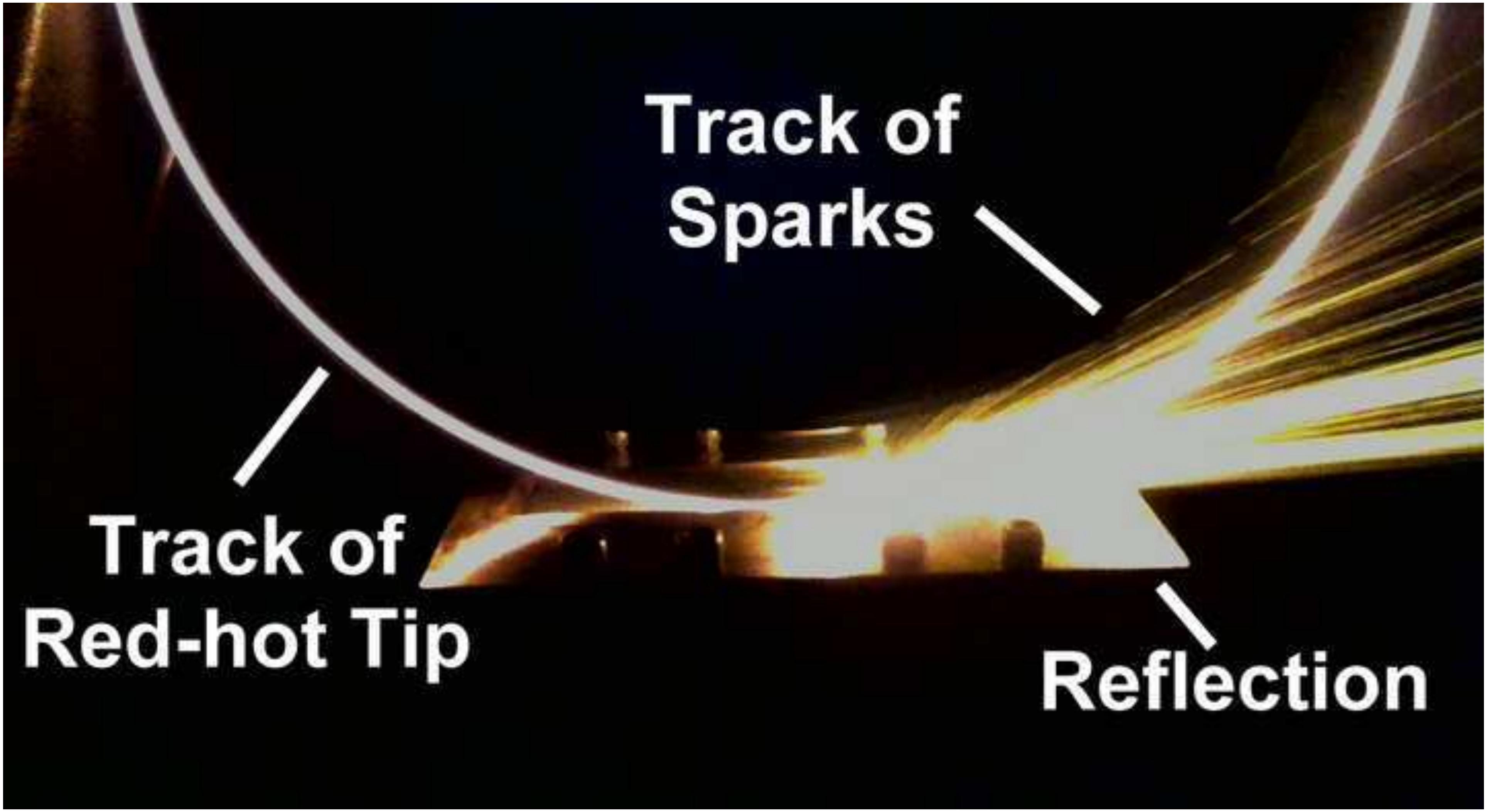

Figure 5

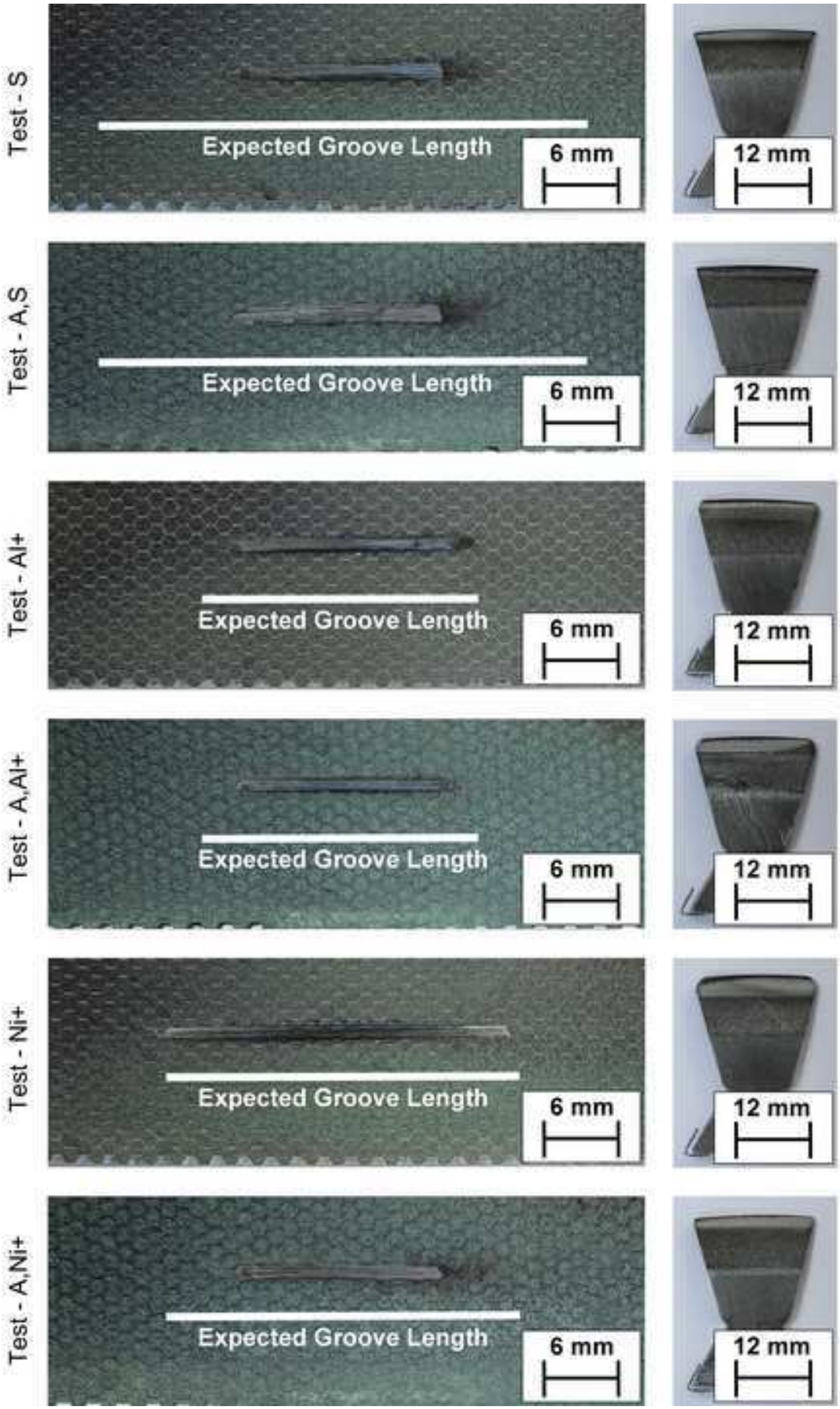
Test - S
Expected Groove Length
6 mm
12 mm
Test - A,S
Expected Groove Length
6 mm
12 mm
Test - Al+
Expected Groove Length
6 mm
12 mm
Test - A,Al+
Expected Groove Length
6 mm
12 mm
Test - Ni+
Expected Groove Length
6 mm
12 mm
Test - A,Ni+
Expected Groove Length
6 mm
12 mm

Figure 6

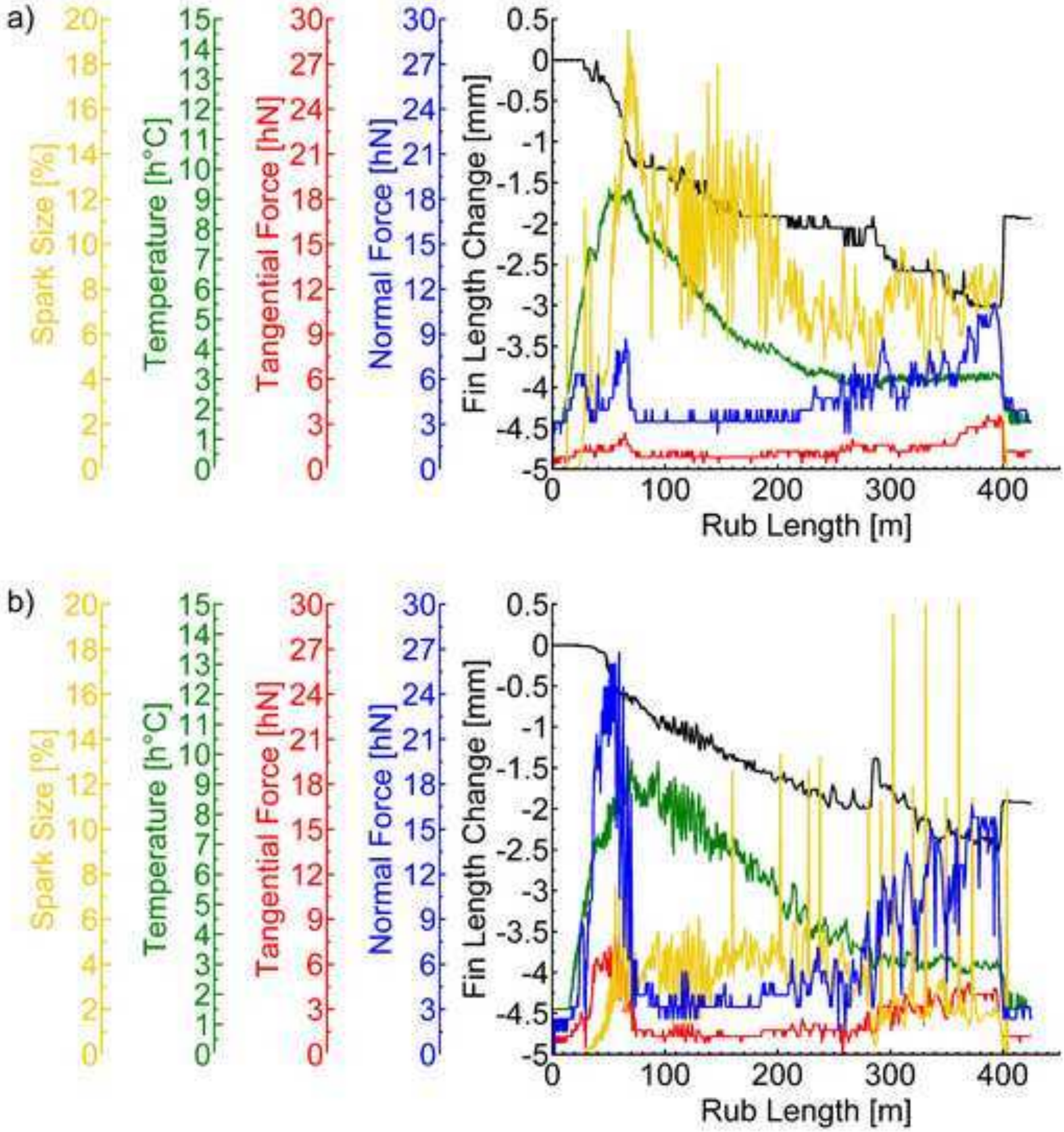

a)
b)
Spark Size [%]
Temperature [h°C]
Tangential Force [hN]
Normal Force [hN]
Fin Length Change [mm]
Rub Length [m]

Figure 7

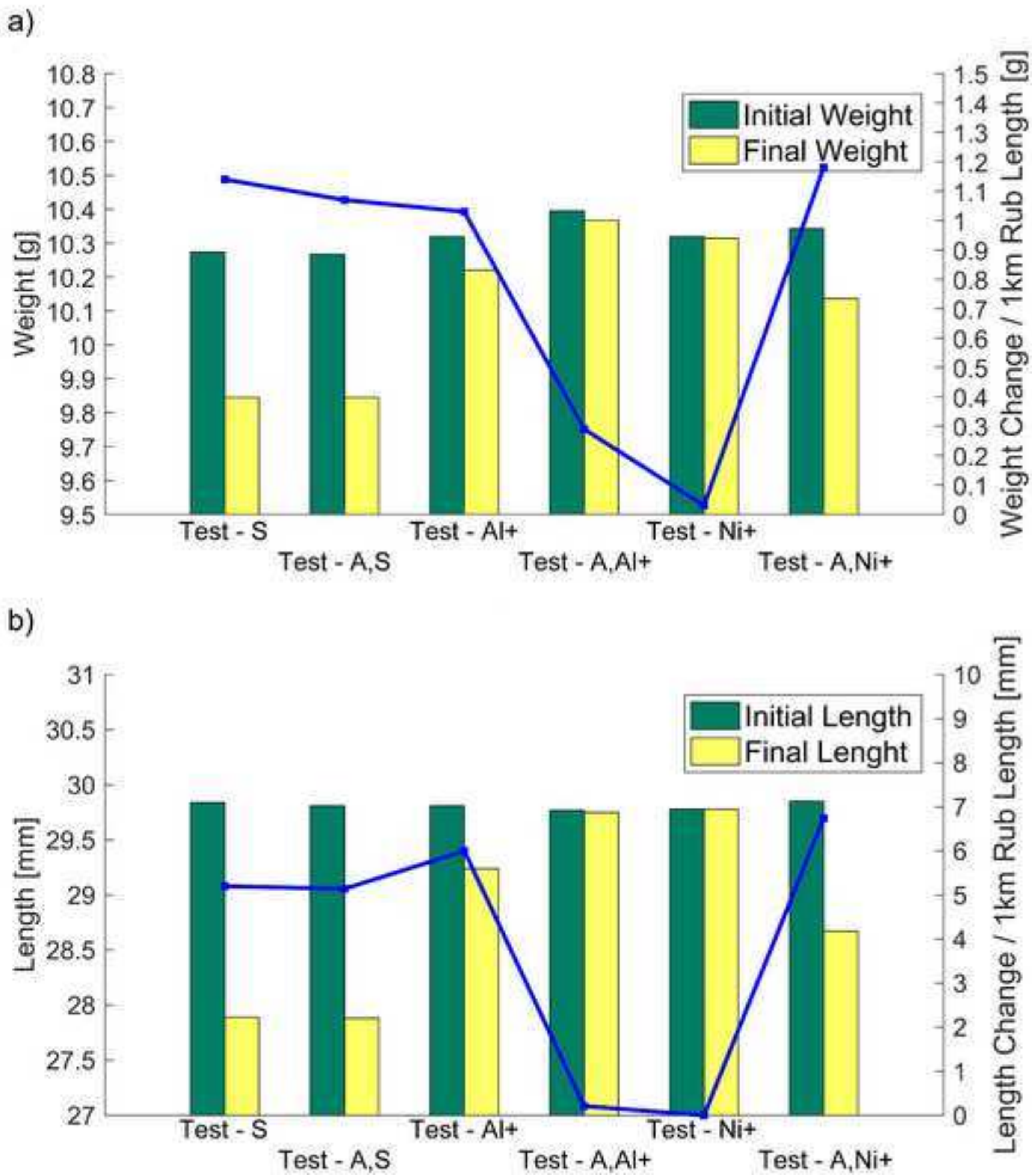

a)
Initial Weight
Final Weight
Weight [g]
Weight Change / 1km Rub Length [g]
10.8
10.7
10.6
10.5
10.4
10.3
10.2
10.1
10
9.9
9.8
9.7
9.6
9.5
1.5
1.4
1.3
1.2
1.1
1
0.9
0.8
0.7
0.6
0.5
0.4
0.3
0.2
0.1
0
Test - S
Test - A,S
Test - Al+
Test - A,Al+
Test - Ni+
Test - A,Ni+
b)
Initial Length
Final Lenght
Length [mm]
Length Change / 1km Rub Length [mm]
31
30.5
30
29.5
29
28.5
28
27.5
27
10
9
8
7
6
5
4
3
2
1
0
Test - S
Test - A,S
Test - Al+
Test - A,Al+
Test - Ni+
Test - A,Ni+

Figure 8

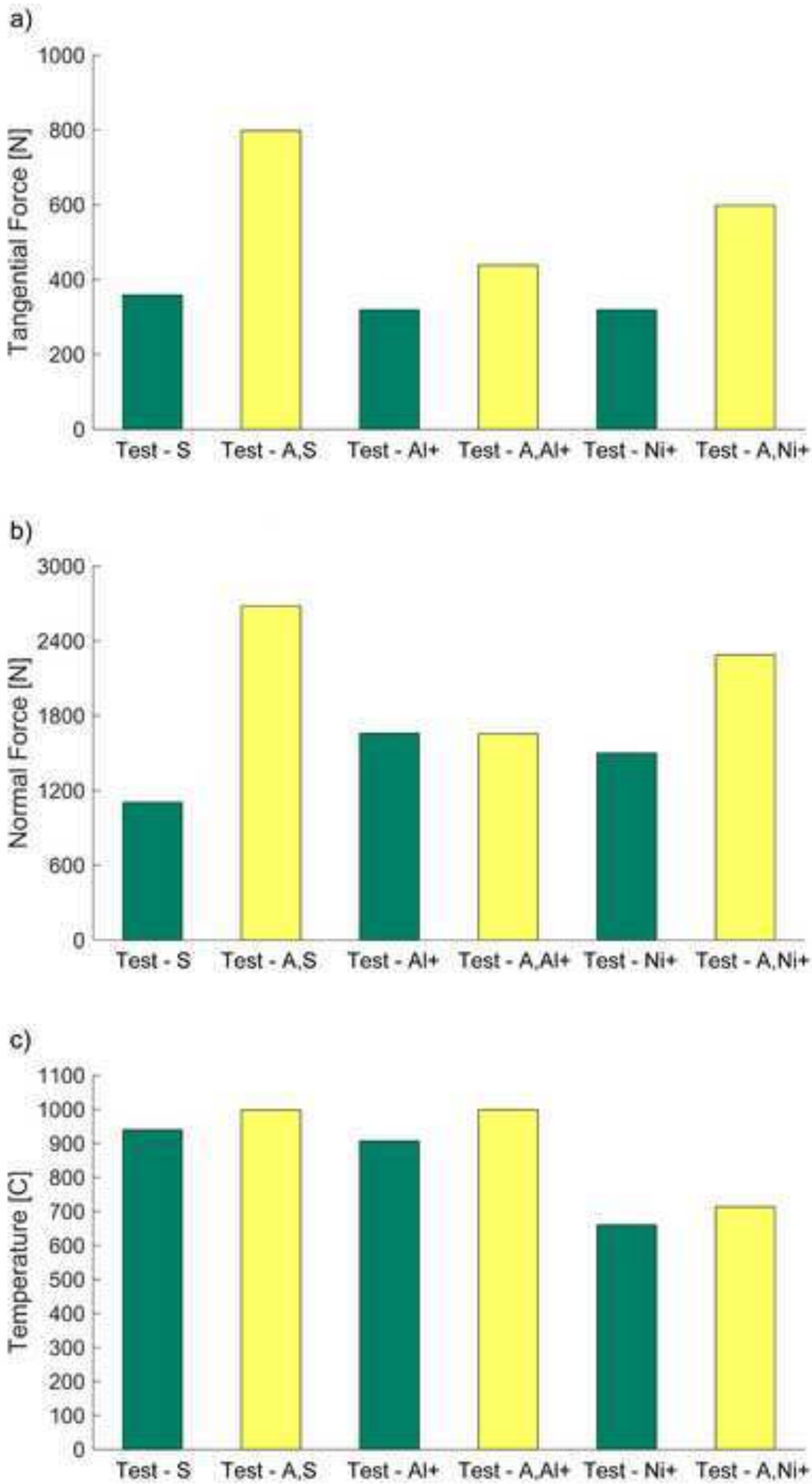
a)
1000
800
600
400
200
0
Tangential Force [N]
Test - S
Test - A,S
Test - Al+
Test - A,Al+
Test - Ni+
Test - A,Ni+
b)
3000
2400
1800
1200
600
0
Normal Force [N]
Test - S
Test - A,S
Test - Al+
Test - A,Al+
Test - Ni+
Test - A,Ni+
c)
1100
1000
900
800
700
600
500
400
300
200
100
0
Temperature [C]
Test - S
Test - A,S
Test - Al+
Test - A,Al+
Test - Ni+
Test - A,Ni+

Figure 9

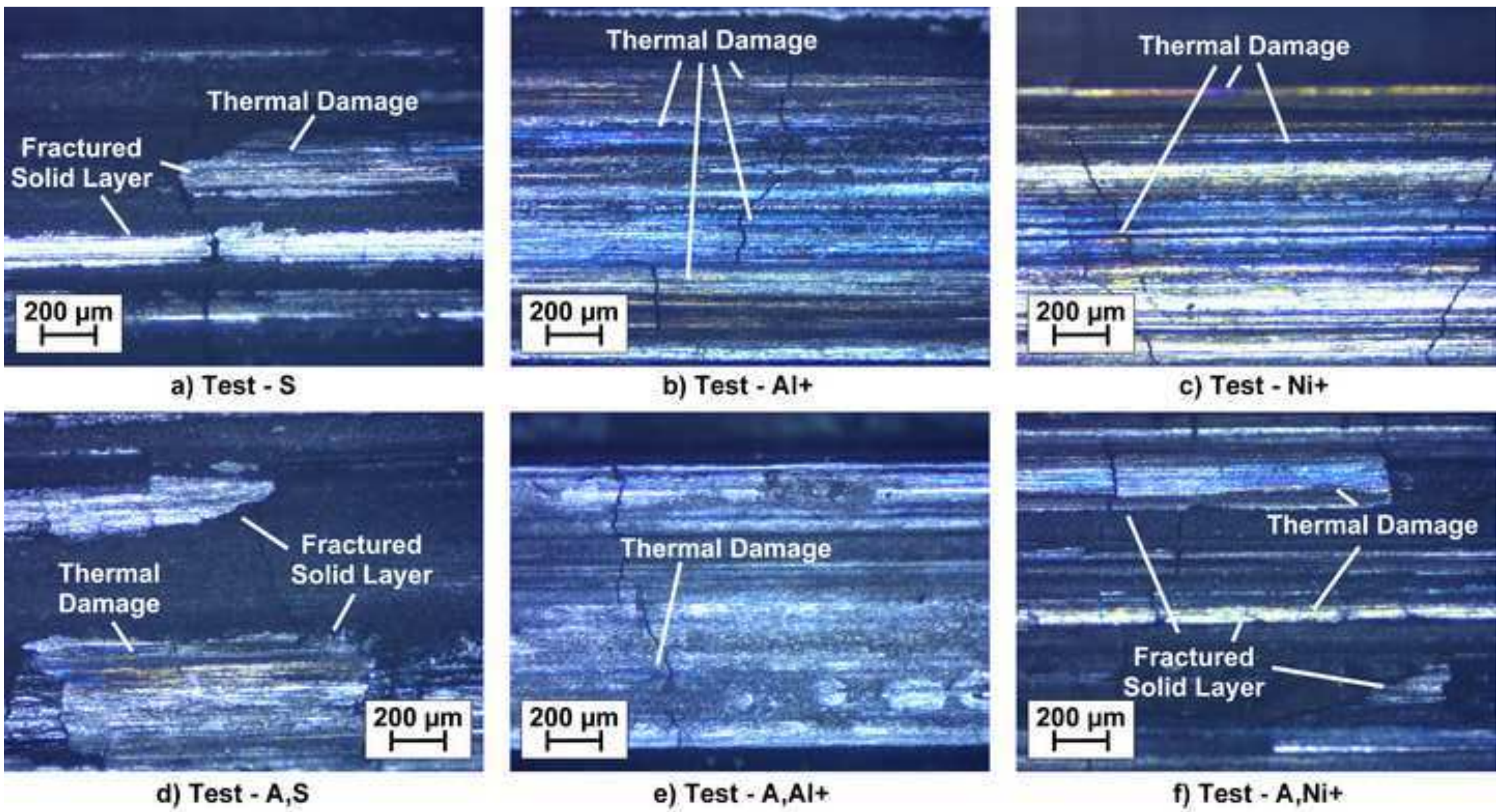

Thermal Damage
Fractured
Solid Layer
200 µm
a) Test - S
Thermal Damage
200 µm
b) Test - Al+
Thermal Damage
200 µm
c) Test - Ni+
Fractured
Solid Layer
Thermal
Damage
200 µm
d) Test - A,S
Thermal Damage
200 µm
e) Test - A,Al+
Thermal Damage
Fractured
Solid Layer
200 µm
f) Test - A,Ni+

Figure 10

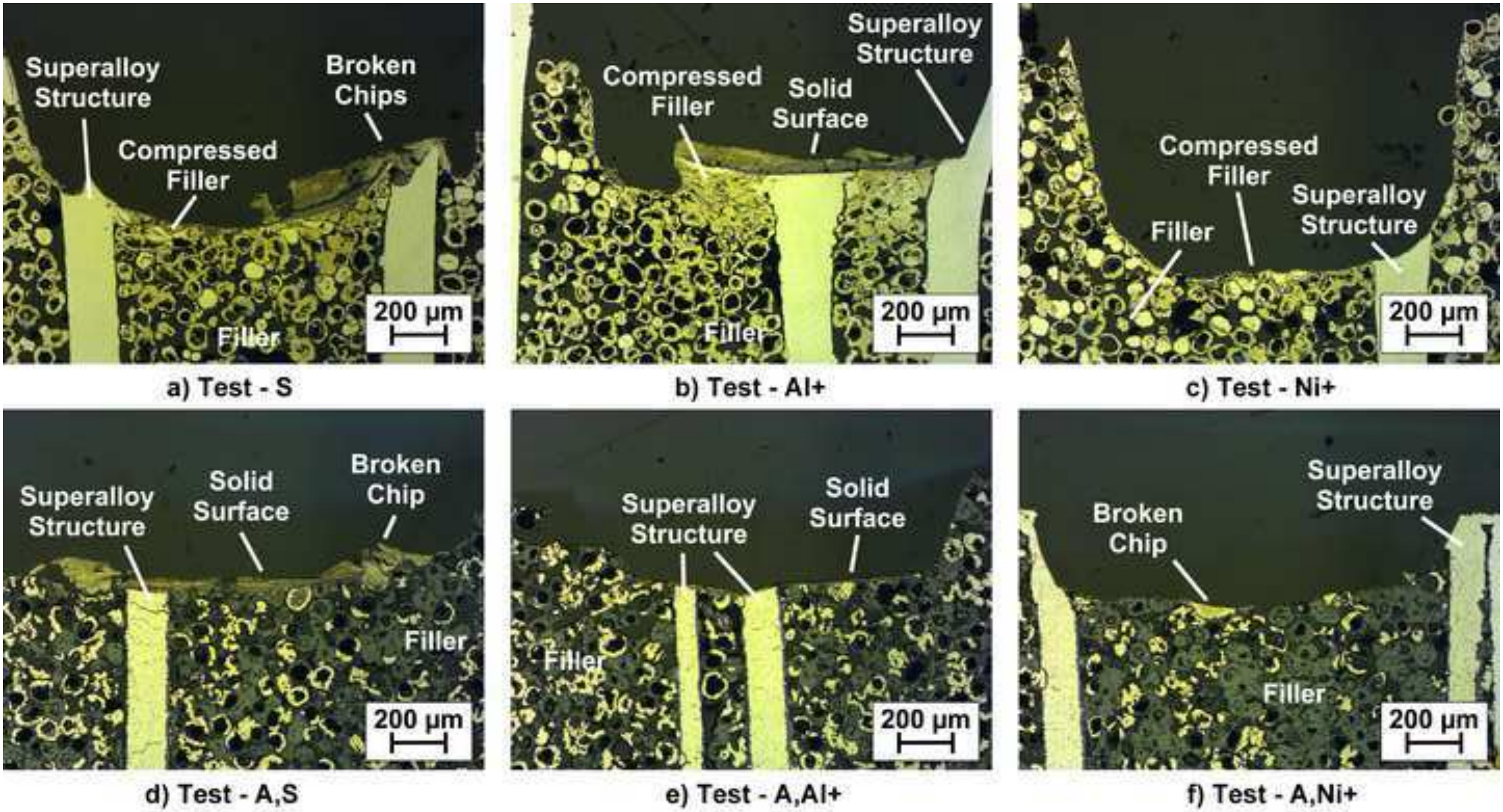

Superalloy Structure
Broken Chips
Compressed Filler
Filler
200 µm
a) Test - S
Compressed Filler
Solid Surface
Superalloy Structure
Filler
200 µm
b) Test - Al+
Compressed Filler
Superalloy Structure
Filler
200 µm
c) Test - Ni+
Superalloy Structure
Solid Surface
Broken Chip
Filler
200 µm
d) Test - A,S
Superalloy Structure
Solid Surface
Filler
200 µm
e) Test - A,Al+
Broken Chip
Superalloy Structure
Filler
200 µm
f) Test - A,Ni+

Figure 11

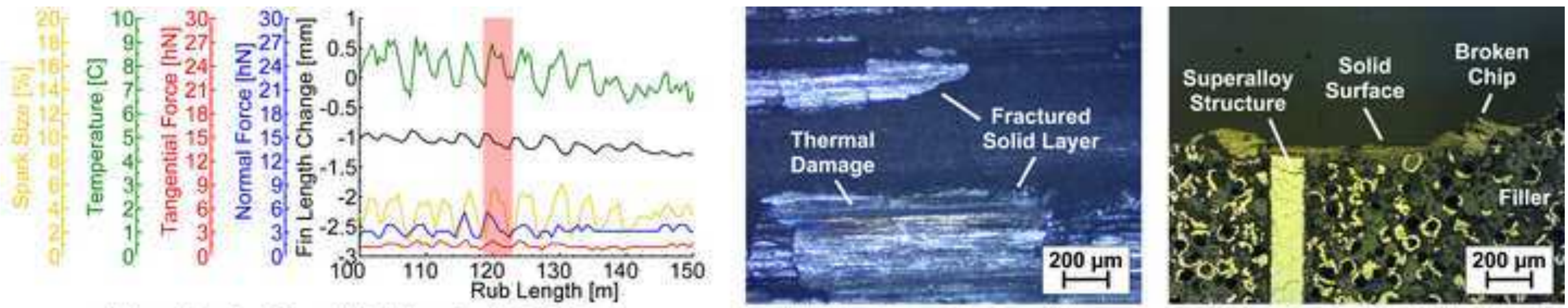

a) Incursion Test Result (Rub Length: 100 - 150 m)

b) Wear Groove Surface View

c) Wear Groove Sectioning View

Table 1

Test Code	Fin Type	Abradable	Tip Speed [m/s]	Incursion speed [μm/s]
Test - S	IN718-HVOF	Standard	200	62.1
Test - A,S	IN718-HVOF	Aged standard	200	62.1
Test - Al+	IN718-HVOF	Aluminium rich	200	62.1
Test - A,Al+	IN718-HVOF	Aged aluminium rich	200	62.1
Test - Ni+	IN718-HVOF	Nickel rich	200	62.1
Test - A,Ni+	IN718-HVOF	Aged nickel rich	200	62.1

Table 2

Test Code	Fin Type	Abradable	Tip Speed [ms-1]	Incursion Rate [µm/pass]	Incursion Depth [µm]
Test - S	IN718-HVOF	Standard	200	0.2	2500
Test - A,S	IN718-HVOF	Aged standard	200	0.2	2500
Test - Al+	IN718-HVOF	Aluminium rich	200	0.2	1000
Test - A,Al+	IN718-HVOF	Aged aluminium rich	200	0.2	<1000
Test - Ni+	IN718-HVOF	Nickel rich	200	0.2	1500
Test - A,Ni+	IN718-HVOF	Aged nickel rich	200	0.2	1500

Table 3

Test Number	Ti	Cr	Fe	Co	Ni[1]	Cu
Test - S	0.81	14.35	17.92	1.21	57.75	0.08
Test - A,S	0.97	18.03	18.09	0.56	53.12	0.09
Test - Al+	0.96	19.74	18.11	0.64	50.22	0.08
Test - A,Al+	1.39	25.16	14.71	1.71	47.89	0.16
Test - Ni+	0.00	3.51	3.34	0.38	90.19	0.06
Test - A,Ni+	0.97	18.23	17.77	1.03	52.03	0.07
Fin Base	0.95	16.69	17.33	0.17	47.53	8.17
Fin Tip	0.00	1.27	0.00	2.61	3.37	0.07
Abradable[2]	0.04	5.36	1.65	0.23	90.46	0.08

[1] FISCHERSCOPE® X-RAY XAN® 250 cannot detect aluminium element therefore the nickel content in the ta

[2] The abradable XRF result present the average value of six different abradable samples